

Prediction of good reaction coordinates and future evolution of MD trajectories using Regularized Sparse Autoencoders – A novel deep learning approach

Abhijit Gupta and Arnab Mukherjee

Department of Chemistry, Indian Institute of Science Education and Research, Pune,
Maharashtra, 411008, India

Abstract:

Identifying reaction coordinates(RCs) is an active area of research, given the crucial role RCs play in determining the progress of a chemical reaction. The choice of the reaction coordinate is often based on heuristic knowledge. However, an essential criterion for the choice is that the coordinate should capture both the reactant and product states unequivocally. Also, the coordinate should be the slowest one so that all the other degrees of freedom can easily equilibrate along the reaction coordinate. Also, the coordinate should be the slowest one so that all the other degrees of freedom can easily equilibrate along the reaction coordinate. We used a regularised sparse autoencoder, an energy-based model, to discover a crucial set of reaction coordinates. Along with discovering reaction coordinates, our model also predicts the evolution of a molecular dynamics(MD) trajectory. We showcased that including sparsity enforcing regularisation helps in choosing a small but important set of reaction coordinates. We used two model systems to demonstrate our approach – alanine dipeptide system and proflavine and DNA system, which exhibited intercalation of proflavine into DNA minor groove in an aqueous environment. We model MD trajectory as a multivariate time series, and our latent variable model performs the task of multi-step time series prediction. This idea is inspired by the popular sparse coding approach - to represent each input sample as a linear combination of few elements taken from a set of representative patterns.

Introduction:

We widely use reaction coordinates throughout chemical physics to model and understand complex chemical transformations. Often simple chemical reactions can be described in terms of one-dimensional reaction-coordinate, which differs from the Cartesian coordinates, and is a generalized coordinate of the system $q = q(r_1, r_2, \dots, r_N)$, a function of cartesian coordinate. For describing a complex dynamical process, it is often necessary to use a set of reaction coordinates. The set of such reaction coordinates themselves comprise a combination of simple reaction coordinates. When generalized coordinates describe a reaction profile, they are typically referred to as reaction coordinates, collective variables (CVs), or order parameters, depending on the context and type of system. Reaction coordinates play a pivotal functional role in understanding the dynamics of a chemical reaction. A good set of reaction coordinates is required to estimate kinetically significant energy barriers or elucidating reaction mechanisms.¹ The natural reaction coordinate is the most informative about the system's future evolution among all different one-dimensional measurements of the state of some high-dimensional dynamical system. While reaction coordinates or collective variables are potentially helpful and intuitively appealing, we must be careful while using them. For example, molecular dynamics (MD) simulation allows us to study molecular processes, but the sampling problem constrains its usefulness. A solution to this long-standing problem is enhanced sampling approaches. However, when applied to poorly chosen reaction coordinates, they can bias the system in misleading ways and generate erroneous predictions of free energy barriers, transition states, and mechanisms. Furthermore, reactions in condensed phase systems occur in a very high dimensional space that includes many uninvolved solutes, solvent coordinates that are not intrinsic to identifying reaction coordinates. Thus, it often leads to several difficulties in deciphering correct reaction coordinates, which renders the use of "physical intuition", or ad-hoc methods routinely employed infeasible and inaccurate.

Even though the idea of reaction coordinate is so widely used in chemical kinetics, the community has not reached a consensus regarding its precise definition.²⁻⁵ In our approach, we wish to define the natural reaction coordinate to not depend on a particular "reaction" or "product" conformations or subsets of phase space.⁶ A natural reaction coordinate should be a function that maps any point in the phase space to a single real number $q: \Omega \rightarrow \mathbb{R}$, where q is the reaction coordinate, and Ω denotes the phase space. The reaction coordinate of this form includes geometric or physical observable properties. Other definitions, mainly the path-based ones such as MEP or MAP, do not take this form. Instead, they define a path through phase

space, a mapping from \mathbb{R} to Ω . These paths map an arc length to phase space coordinate. The reaction coordinate's value is undefined for all conformations in Ω that are not on the path.

In our approach, we jointly predict the optimal set of physically interpretable reaction coordinates and the future evolution of the dynamical system. We model the MD trajectories, which are input in our machine learning(ML) model as a collection of multivariate time series(MTS).

Also, the coordinate should be the slowest one so that all the other degrees of freedom can easily equilibrate along the reaction coordinate⁷. Previous work involved using Principal component analysis(PCA), a technique used for dimensionality reduction, to approximate reaction coordinates. The problem with PCA is that it does not consider the time aspect involved in MD trajectory data. It chooses the direction of maximum variance, which is usually not what we are looking for when searching for slow coordinates⁸. Another factor that limits the applicability of PCA is that different low dimensional representations constructed by PCA are not comparable with each other. We might choose different sets of internal coordinates, like contact distances, bond dihedrals, and each yields a different solution. Sultan et al. used time-structured based independent component analysis(tiCA) for identifying RCs. tiCA aims to find projections of the MD data that minimise the loss of kinetic information. Unlike PCA, tiCA does not assume that high variance modes are associated with slow degrees of freedom. It does so by maximising the autocorrelation function. However, tiCA is a linear model, and this limits its ability. Kernel trick can be used to extend tiCA and yield non-linear solutions. However, it is computationally expensive and is dependent on tuning and choice of kernel⁹. There have been several deep learning-based approaches for choosing or discovering an optimal set of reaction coordinates in recent times. VAMPnets employ the variational approach for Markov processes (VAMP) to develop a deep learning framework for molecular kinetics using neural networks. It encodes the entire mapping from molecular coordinates to Markov states, thus combining the whole data processing pipeline in a single end-to-end framework¹⁰. Wehmeyer et al. used a variant of autoencoder, namely time-lagged autoencoder, to find low dimensional embeddings for the high dimensional molecular dynamics data¹¹. They highlighted the importance of using an appropriate set of collective variables(CVs) in Markov state modelling(MSM) and employed their approach on different analytical systems and alanine dipeptide systems. The Variation approach for conformation dynamics(VAC) forms

the basis of many methods that are currently used for identifying slow CVs¹². It searches for d orthogonal directions r_i , such that the projection $r_i^T z_t$ is maximal. The eigenvalues of the propagator bound these autocorrelations from above. Nuske et al. emphasized that the eigenvalues and eigenvectors of the MD propagator, also called the transfer operator, contain the key information about thermodynamics and kinetics. They presented a variational approach for the calculation of the dominant eigenvectors and eigenvalues of the propagator. In the Markovian model-based approach, there is an implicit assumption that the future evolution of the system, $x_{t+\tau}$ depends only on the present state x_t , where t is the time step and τ is the lag time. There are many physical processes, both deterministic and stochastic, which are Markovian.

Dynamic mode decomposition(DMD) is another approach for finding RCs. It tries to minimise the regression error: $\sum_t \|z_{t+\tau} - \mathbf{K}^T z_t\|^2$, where \mathbf{K} is a linear model, and compute its d eigenvectors r_i with largest eigenvalues^{13,14}. All these models use a linear model of the form:

$$\mathbb{E}[g(x_{t+\tau})] = K^T \mathbb{E}[f(x_t)]$$

The $f(\cdot)$ and $g(\cdot)$ are feature transformations that act on x and transform it into the feature space where dynamics are approximately linear. The expectation value over the time accounts for the stochasticity. For DMD, the feature transformation is an identity transformation \mathbb{I} .

Dimension reduction can be facilitated when working feature space instead of directly using the cartesian coordinates¹⁵.

Methods

We denote a matrix of multivariate time series by \mathbf{X} and its component column vectors by \mathbf{x} . For a vector \mathbf{x} , its i -th element is denoted by x_i . For a matrix \mathbf{X} , we use x_i as the i -th column and $x_{i,j}$ is the (i,j) -th entry of \mathbf{X} . In our model, we denote a collection of high dimensional multivariate time series by $(\mathbf{x}_{T+1}, \dots, \mathbf{x}_{T+k})$, where each \mathbf{x}_i is a vector of dimension n (features) at time point i . Here, T , denotes an arbitrary time point. We consider the problem of forecasting l time future values, given the information(history) about $(k - l)$ time steps. The \bar{y} denotes the reconstructed future output (windowed trajectory). We now outline below the architecture of a

simple autoencoder and highlight the difference between it and our modified sparse autoencoder that uses additional regularization terms.

A simple autoencoder is trained to reconstruct the input fed to it. It consists of an encoder and a decoder function [Figure 1].

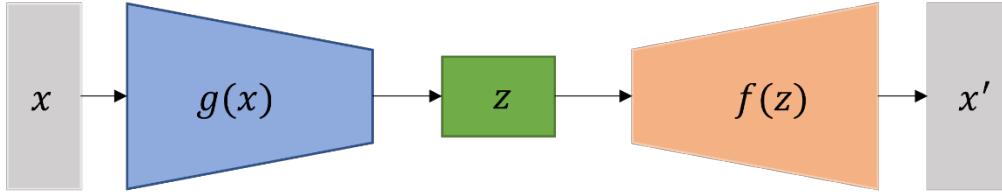


Figure 1: A schematic representation of a simple autoencoder. The code or the latent vector z is not regularized, and the auto-encoder can be made over-complete or under-complete by tuning the dimension of z .

The encoder function $g(\cdot)$ takes the input x and learns the mapping $x \rightarrow z$, where z denotes the latent space representation of x . The z is also called the latent vector since it consists of latent or "hidden" values that are not observed in the data. The decoder function $f(\cdot)$ learns the mapping $z \rightarrow x$ and outputs x' , which is called the reconstructed input. The loss function for such an architecture is the reconstruction error measured as the mean squared error(MSE) between the original input x and the reconstructed input x' .

Our regularized sparse autoencoder architecture accepts as an input a multivariate time series x_t and instead of simply reconstructing the input, it predicts the $x_{t+\tau}$, i.e. the evolution of the trajectory x_t after lag time τ . As mentioned earlier, we denote the prediction by \bar{y} .

The loss function for our model is the sum of three terms. \mathbf{C} measures the reconstruction error between the output and the model prediction. \mathbf{R} is the sparsity regularisation term for the latent variable \mathbf{z} . Here, we impose the \mathbf{L}_1 regularizer on the latent variable. L_2 is the ridge penalty $\lambda \sum_{j=1}^d z_j^2$ and L_1 is the lasso penalty $\lambda \sum_{j=1}^d |z_j|$ that we have used in our regularization function \mathbf{R} on the latent vector for the loss function.

The motivation behind using \mathbf{L}_1 regularization is that in a high dimensional space, many of the weight parameters will equal zero simultaneously. Intuitively, it helps in choosing those latent variables which contribute significantly towards the prediction of the evolution of an MD trajectory. This scenario is quite unlike the \mathbf{L}_2 regularization, which does not impose a sparsity

constraint, i.e., it encourages the weight values towards zero (but not exactly zero). \mathbf{D} is the error associated with Encoder prediction of latent variable $\bar{\mathbf{z}}$ and \mathbf{z} :

$$\text{Loss} = \mathcal{C}(y, \text{Dec}(z, h)) + \mathbf{D}(\mathbf{z}, \text{Enc}(y, h)) + \lambda \mathbf{R}(z)$$

The addition of an additional sparsity regularizer forces the autoencoder to cut down the number of active neurons in the coding layer. This results in representation generated by combination of a small number of active neurons. An alternative strategy is to actually measure the sparsity of the coding layer and penalize the model when this exceeds the target value of sparsity. If we want to measure the divergence between the target threshold(probability) p that a neuron in the coding layer will activate and the actual probability q , we can measure the KL divergence.

$$D_{KL}(p \parallel q) = p \log \frac{p}{q} + (1 - p) \log \frac{1 - p}{1 - q}$$

In the current approach, though, we have chosen L_1 regularization.

By varying the latent variable in the latent space, the output generated varies over the manifold of possible predictions. This provides the model with the ability to make multimodal prediction. The model finds the optimal z that minimizes the reconstruction error. The regularization constraints on z limit its information capacity and forces the model to learn non-trivial latent space representation of the inputs. In an energy-based modelling terminology, this limits the volume of space that has low energy¹⁶.

To update the parameters of the model, we first predict z that minimizes

$$\mathcal{C}(y, \text{Dec}(z, h)) + \lambda \mathbf{R}(z),$$

and then use this z as a feedback signal (target) that predicts $\bar{\mathbf{z}}$ from x and y (Figure 2, greyed box) by feeding h and y into the *Encoder* with $D(z, \bar{z})$ as the loss. This strategy helps in learning optimal z , and we do not have to make the latent variable inference again.

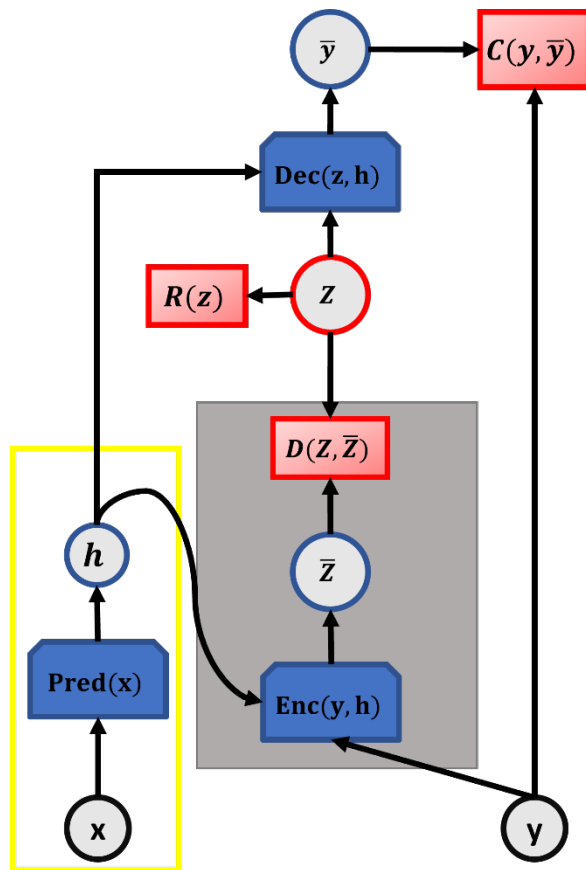


Figure 2: A schematic representation of our architecture. The greyed box contains the Encoder that predicts \bar{z}

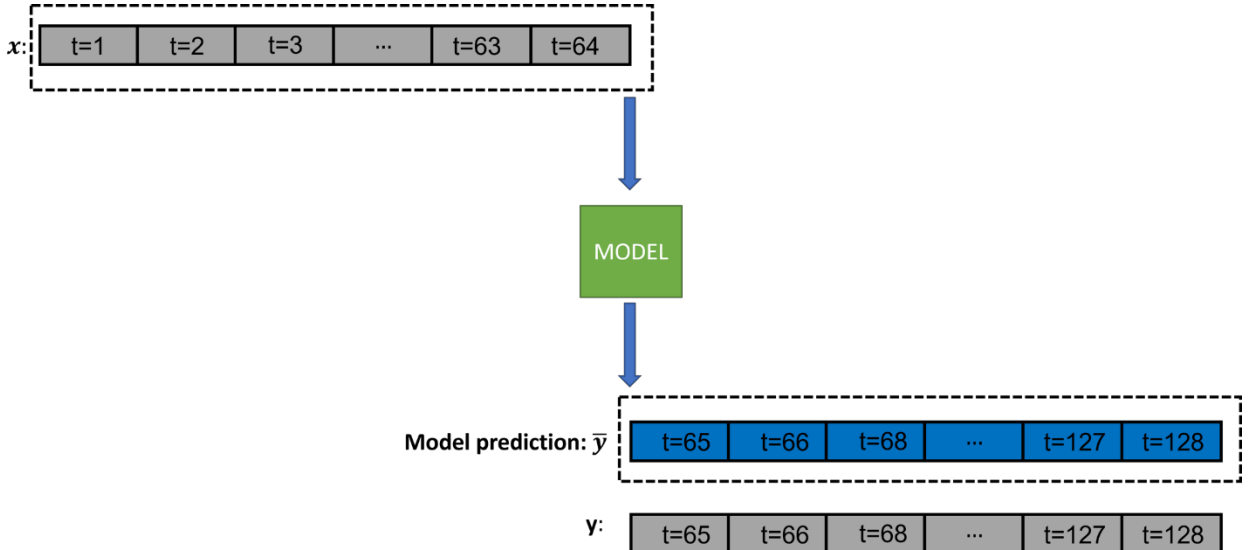


Figure 3: A schematic representation of data flow – our multi-step prediction model predicts \bar{y} vector of length l .

We train our model end-to-end to predict optimal sparse latent variable z (Reaction coordinate(s)), along with future values $y := x_{T+k-l+1:T+k} = \{x_{T+k-l+1}, \dots, x_{T+k}\}$ based on the past $k - l$ steps $\{x_{T+1}, x_{T+2}, \dots, x_{T+k-l}\}$. T denotes the starting point in the data (Figure 3)

We applied our model to the two systems –

- 1) Study of different metastable states of alanine dipeptide
- 2) Intercalation of Proflavine into DNA minor groove in an aqueous environment¹⁷

For the alanine dipeptide system, we retrieved data from two sources:

1. We used MDSHARE¹⁸ to obtain MD simulation data, consisting of 250ns trajectories spanning all 6 metastable states. The details of the trajectories are given below in Table 1.

Table 1: MD trajectory details

Property	Value
Code	ACEMD
Forcefield	AMBER ff-99SB-ILDN

Integrator	Langevin
Integrator time step	2 fs
Simulation time	250 ns
Frame spacing	1 ps
Temperature	300 K
Volume	(2.3222 nm) ³ periodic box
Solvation	651 TIP3P waters
Electrostatics	PME
PME real-space cutoff	0.9 nm
PME grid spacing	0.1 nm
PME updates	every two-time step
Constraints	all bonds between hydrogens and heavy atoms

2. **shoot-302K-100ps:** This dataset contains 5000 x 100 ps shooting trajectories out of each of 6 manually-identified states. Hamiltonian trajectories (velocity Verlet without thermostat) were initiated from a canonical (NVT) distribution at 302 K from within each state¹⁹.

We used PyEMMA¹⁸ and extracted backbone torsions, backbone atom positions, and backbone atom distances for the featurization of the data. This results in three feature matrices of dimensions (T, 11), (T, 4), and (T, 18), respectively for a single trajectory. The time series data is represented as a tensor, with batch dimension as the first axis (Figure 4)

We adopt the following data windowing strategy:

Our model involves multi-output and multi-time step prediction. Figure 3 shows a schematic representation of single output, multi-output prediction. We used a window size of 128. The output size is also 128 in length.

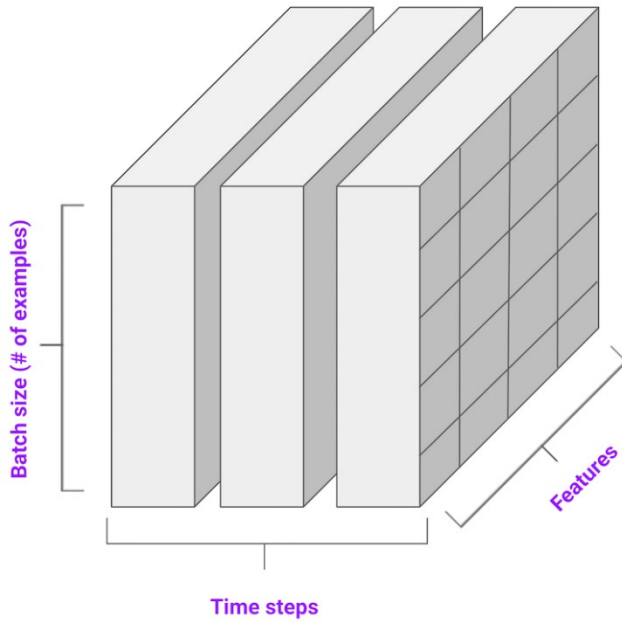


Figure 4: representing multivariate time series data – a tensor of shape : (Number of examples, time steps, features). For a single sample, the batch axis can be ignored.

We have used stacked 1D convolutional layers, doubling the dilation rate at every layer. The receptive field doubles at every layer. This architecture is similar to wavenet.²⁰ The lower layers in the encoder learn short-term patterns, and the higher layers learn long term patterns. Doubling of dilation rate at each layer gives the network the ability to handle very long sequences.

The decoder architecture is symmetric with the encoder and uses dilated deconvolutions and is defined by transposed operations. The loss used for \mathbf{D} and \mathbf{Z} is MSE.

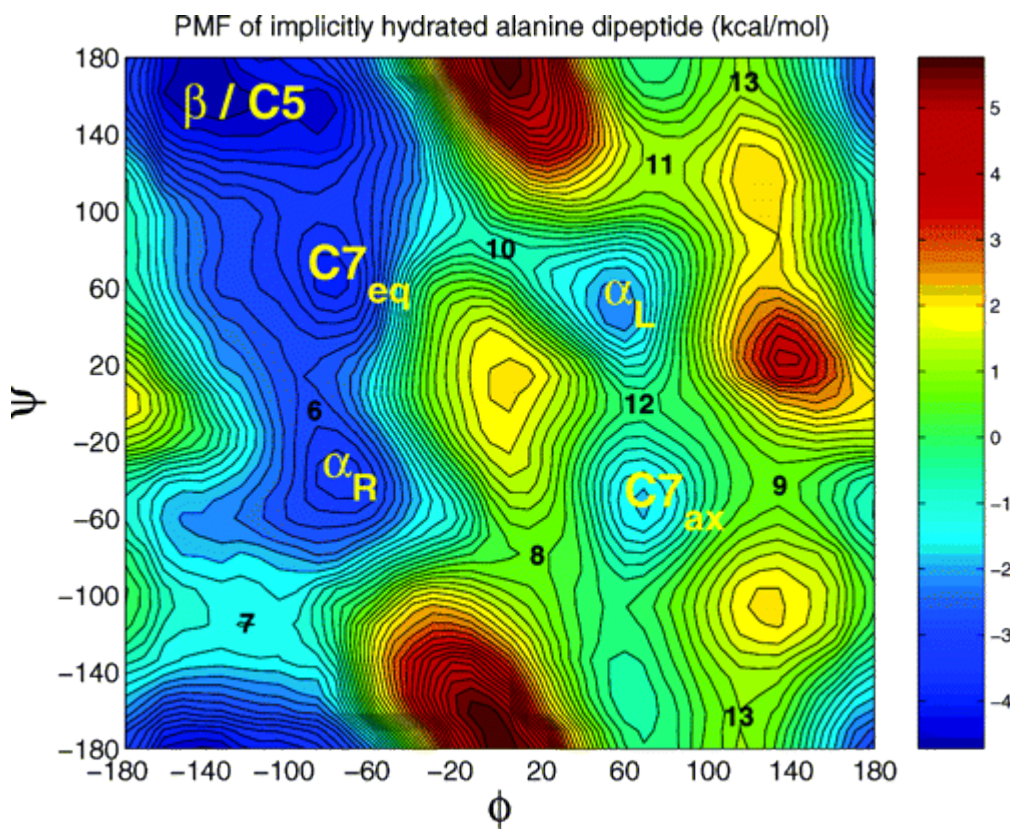


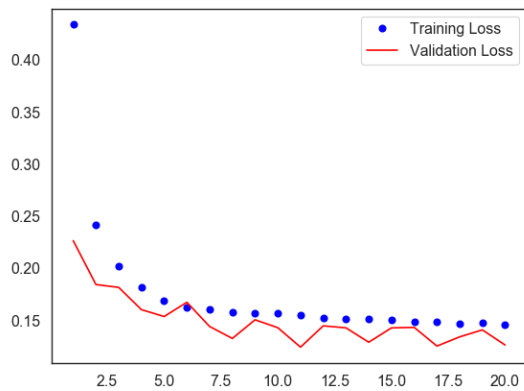
Figure 5: Contour map of the interpolated PMF of the implicitly hydrated alanine dipeptide. Adapted with permission from Long-Time Conformational Transitions of Alanine Dipeptide in Aqueous Solution: Continuous and Discrete-State Kinetic Models; Dmitriy S. Chekmarev, Tateki Ishida, and Ronald M. Levy; *The Journal of Physical Chemistry B* **2004** *108* (50), 19487-19495; DOI: 10.1021/jp048540w. Copyright 2004 American Chemical Society

The different metastable states of alanine dipeptide are shown in Figure 5.

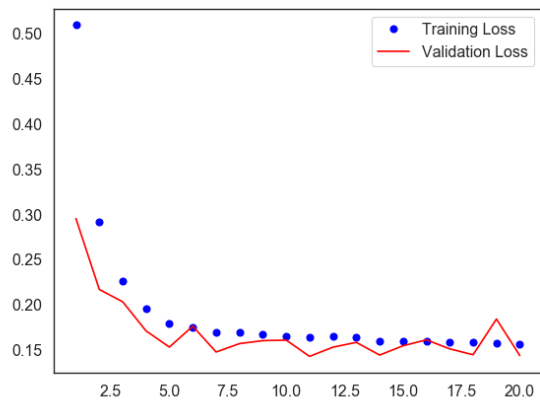
The main conformers of the hydrated alanine dipeptide molecule can be arranged in the following order according to the effective free energy difference ΔW with respect to the lowest energy structure $\beta/C5:\beta/C5$ (taken as zero energy) $< C7_{eq} (\Delta W \approx 0.9 \text{ kcal/mol}) < \alpha_R (\Delta W \approx 1.5 \text{ kcal/mol}) < \alpha_L (\Delta W \approx 2.7 \text{ kcal/mol}) < C7_{ax} (\Delta W \approx 3.2 \text{ kcal/mol})^{21}$.

In Figure 6, we show the results obtained for the prediction of the future evolution of trajectory for the three features backbone atomic positions, torsions, and distances between atoms. The training and validation loss decreases with each epoch.

(a)



(b)



(c)

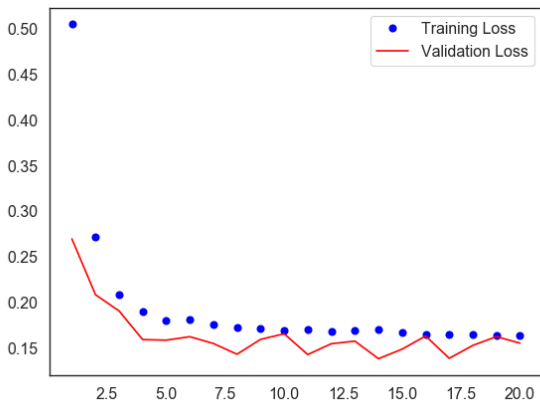


Figure 6: (a) Training and validation loss for prediction of the average of backbone atom positions (b) Training and validation loss for prediction of the average of torsions (c) Training and validation loss for prediction of the average of distances over all atoms

For alanine dipeptide, the torsion angles ϕ and ψ aptly describe its dynamics as it transitions into different metastable states. We used the latent variable representation from our model and compared it with the actual values of the torsions. We observed close agreement between the two (Figure 7).

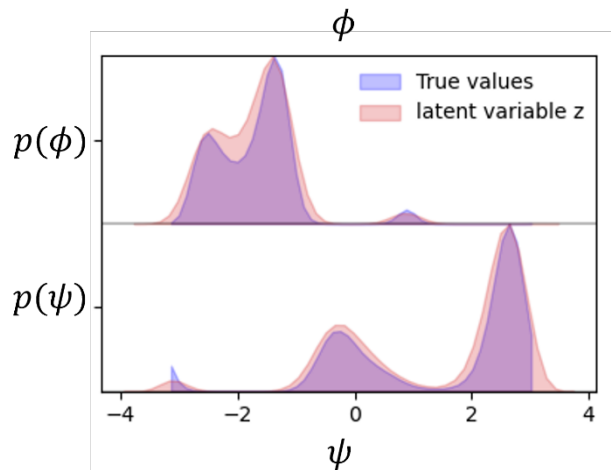


Figure 7: The model predicts the optimal set of latent variables ϕ and ψ as the true reaction coordinates. We have projected the latent variable z found by the model onto the known values of ϕ and ψ . The model's prediction matches closely with the experimentally known reaction coordinates.

For the second system of DNA-proflavine, which describes the phenomenon of recrossing behaviour of MD trajectories near the transition state, the proflavine drug intercalates into the minor groove of DNA in an aqueous environment¹⁷. Recrossing occurs due to the coupling of environment degrees of freedom with the RCs. In this model, we wanted to understand what the key reaction coordinates besides X and φ are near the transition state region for understanding recrossing behaviour. Previously, in our group, we studied the recrossing behaviour by using X (separation) and φ as the reaction coordinates²². While X defines the position of the drug with respect to the intercalation base pairs, the collective variable φ denotes the position of the drug along the helical axis of the DNA. The RR trajectory(described below) are the trajectories that show recrossing behaviour. The different features in DNA are listed in figure 8. The other features are the number of hydrogen bonds between water molecules and proflavine(hbnum1), the number of water around the drug(wat_0.34_flv_heavy) and around the intercalating base-pair IBP (wat_0.34_ibp_heavy), each within 0.34 nm distance, and the separation coordinate¹⁷.

The system details are as follows:

- Tensor of shape (Samples, Timesteps, Features)

1. Reactant – Reactant trajectories (RR) shape: (1050, 6001, 19)
2. Reactant – Product trajectories (RP) shape: (810, 6001, 19)

For training and prediction, we choose the window size of 128 steps. The training phase involves using the windowed trajectory and predicting whether the trajectory will show recrossing behaviour. Figure 9 shows the training and validation accuracy of the model.

Figure 10 shows the SHAP summary plot²³ of each feature and its weightage in its contribution towards the RCs set. The features were inferred by doing canonical correlation analysis(CCA) of encoded time series and univariate time series of each feature. We observed that base pair rise and role parameters contribute the most.

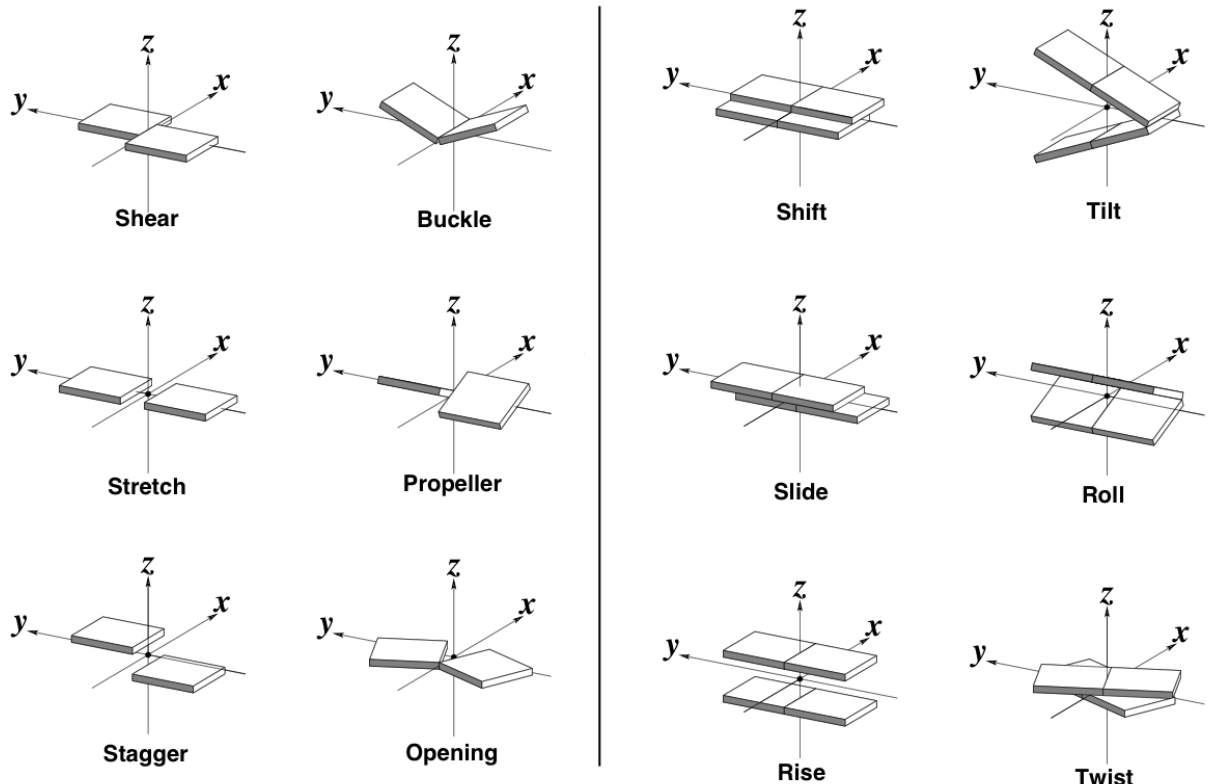


Figure 8: The different translational base pair parameters: Rise, Shift and Slide. The rotational base pair parameters: Twist and Roll. Buckle is a rotational base step parameter. The figure is adapted from article ²⁴ [Lu XJ, Olson WK. 3DNA: a software package for the analysis, rebuilding and visualization of three-dimensional nucleic acid structures. Nucleic Acids Res. 2003 Sep 1;31(17):5108-21. doi: 10.1093/nar/gkg680. PMID: 12930962; PMCID: PMC212791.]

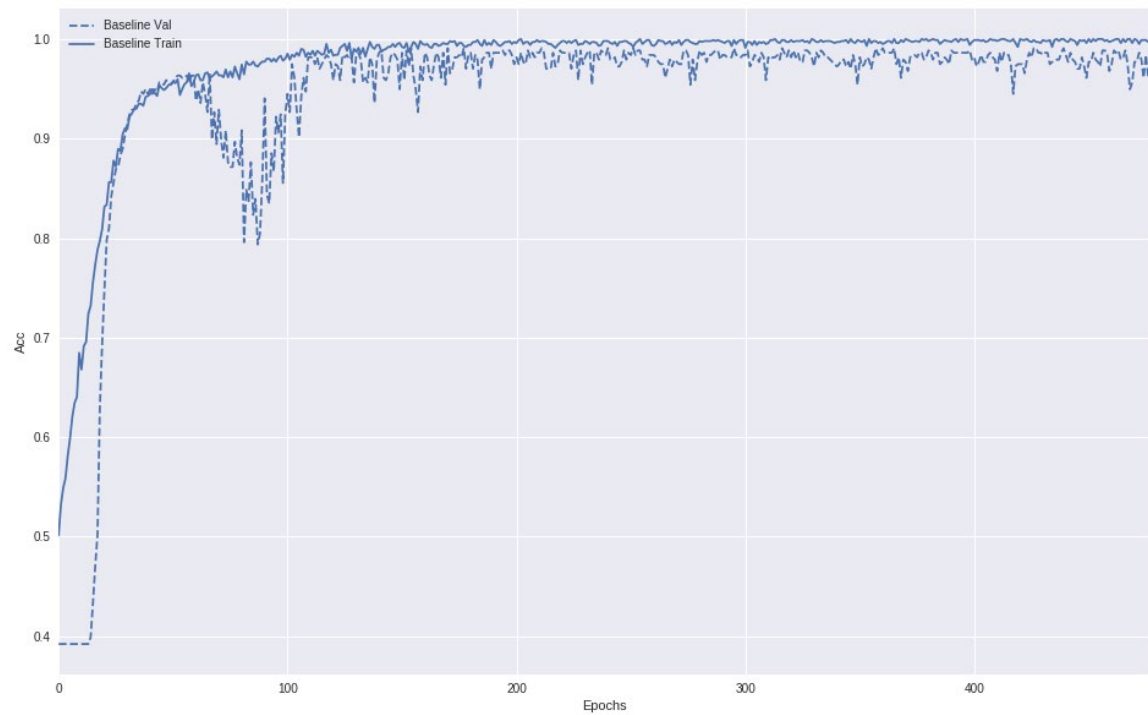


Figure 9: Training and validation accuracy for the DNA-proflavine system

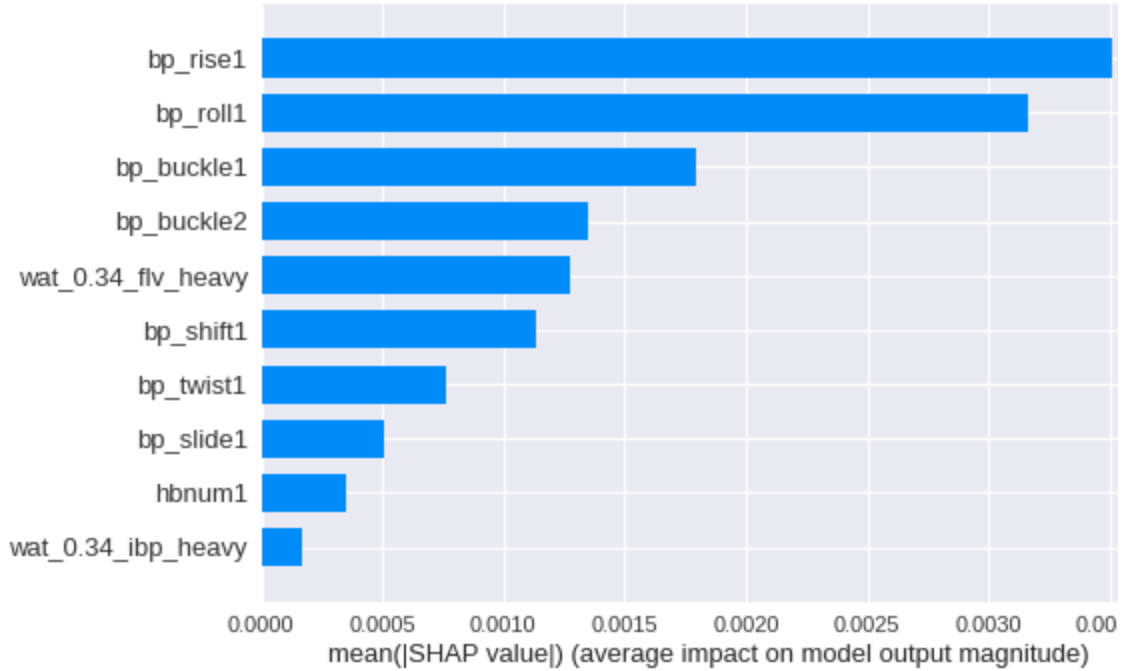


Figure 10: Feature vector importance near the transition state region

In the present study, we intended to study what other factors intrinsic to DNA – rise, roll, shift, buckle, twist, and the number of hydrogen-bonded pairs of water in the vicinity contribute to optimal CV. This was one of the unanswered but crucial questions in the previous study¹⁷.

Discussion and conclusion

Comparison with contemporary approaches

Our method, illustrated in Figure 2, differs from the “time-lagged autoencoder” by Noe et al. in several ways. Firstly, our approach takes inspiration from “Energy-based models” introduced by Yann LeCun et al. and his colleagues¹⁶ and its application in fast sparse coding using autoencoders²⁵. The energy-based model framework was quite revolutionary. For a given input, sparse coding minimizes a quadratic reconstruction error with an L_1 penalty term on the code.

The sparse encoding approach aims to find the **fixed point** of our parametric estimate of the optimal latent vector (reaction coordinate/CVs) $z(t + \tau) = \Theta(\text{Enc}(y, h)_t)$, where Θ is some function that is learned as we train the model by feeding in the widowed trajectories from the

input. $Enc(y, h)_t$ is the encoder output at time t. The idea of finding the fixed point comes from the fact that CVs usually represent the slowest relaxing degrees of freedom⁷, so as the model gets better at each epoch (loss declines, figure 6 and figure 9), the CVs that are learnt get better.

Notably, Noe. et.al. optimize a different objective function (Equation 2)¹¹. Although they have used the same letter **z**, the **z** in their paper is the input trajectory, whereas in our notation **z** represents the latent vector. They have tried to minimize the regression error of reconstruction without sparsity constraints.

In the present study of DNA-drug recrossing for the second system, we intended to study what other factors intrinsic to DNA – rise, roll, shift, buckle, twist, and the number of hydrogen-bonded pairs of water in the vicinity contribute to optimal CV for the recrossing phenomenon. The free energy surface for the DNA-proflavin system is represented in the cited paper from our group¹⁷ in collaboration with Hynes – “Dynamical Recrossing in the Intercalation Process of the Anticancer Agent Proflavine into DNA”. The reaction coordinate for this system was established in ²⁶. Previously, in our group, we studied the recrossing behaviour by using X (separation) and φ as the reaction coordinates²². While X defines the position of the drug with respect to the intercalation base pairs, the collective variable φ denotes the position of the drug along the helical axis of the DNA. This was one of the unanswered but crucial questions in the previous study. For the first specimen in our study(alanine-dipeptide), we already showed the derived CVs and compared it with well-established CVs for that system.

The sparsity constrain in our model limits the model to learn only crucial features ranked by their importance in SHAP graph (Figure 10).

Our strategy of using the latent vector representations can be used to assess and infer the reaction coordinates. As a side effect, the system is also able to predict the future evolution of MD trajectories, which is analogous to time series prediction.

References

- (1) McGibbon, R. T.; Pande, V. S. *J Chem Phys* **2015**, *142*, 124105.
- (2) Fukui, K. Formulation of the Reaction Coordinate. *J. Phys. Chem.* **1970**, *74* (23), 4161–4163.
- (3) Tachibana, A.; Fukui, K. *Theor Chim Acta* **1980**, *57*, 81.
- (4) Quapp, W.; Heidrich, D. *Theor Chim Acta* **1984**, *66*, 245.
- (5) Yamashita, K.; Yamabe, T.; Fukui, K. *Chem Phys Lett* **1981**, *84*, 123.

(6) McGibbon, R. T.; Husic, B. E.; Pande, V. S. Identification of Simple Reaction Coordinates from Complex Dynamics. *J. Chem. Phys.* **2017**, *146* (4), 044109. <https://doi.org/10.1063/1.4974306>.

(7) M. Sultan, M.; Pande, V. S. TICA-Metadynamics: Accelerating Metadynamics by Using Kinetically Selected Collective Variables. *J. Chem. Theory Comput.* **2017**, *13* (6), 2440–2447.

(8) Li, W.; Ma, A. Recent Developments in Methods for Identifying Reaction Coordinates. *Mol. Simul.* **2014**, *40* (10–11), 784–793.

(9) Schwantes, C. R.; Pande, V. S. Modeling Molecular Kinetics with TICA and the Kernel Trick. *J. Chem. Theory Comput.* **2015**, *11* (2), 600–608.

(10) Mardt, A.; Pasquali, L.; Wu, H.; Noé, F. VAMPnets for Deep Learning of Molecular Kinetics. *Nat. Commun.* **2018**, *9* (1), 5. <https://doi.org/10.1038/s41467-017-02388-1>.

(11) Wehmeyer, C.; Noé, F. Time-Lagged Autoencoders: Deep Learning of Slow Collective Variables for Molecular Kinetics. *J. Chem. Phys.* **2018**, *148* (24), 241703. <https://doi.org/10.1063/1.5011399>.

(12) Nuske, F.; Keller, B. G.; Pérez-Hernández, G.; Mey, A. S.; Noé, F. Variational Approach to Molecular Kinetics. *J. Chem. Theory Comput.* **2014**, *10* (4), 1739–1752.

(13) Mezić, I. Spectral Properties of Dynamical Systems, Model Reduction and Decompositions. *Nonlinear Dyn.* **2005**, *41* (1), 309–325.

(14) Tu, J. H. Dynamic Mode Decomposition: Theory and Applications. **2013**.

(15) Harrigan, M. P.; Sultan, M. M.; Hernández, C. X.; Husic, B. E.; Eastman, P.; Schwantes, C. R.; Beauchamp, K. A.; McGibbon, R. T.; Pande, V. S. MSMBuilder: Statistical Models for Biomolecular Dynamics. *Biophys. J.* **2017**, *112* (1), 10–15.

(16) LeCun, Y.; Chopra, S.; Hadsell, R.; Ranzato, M.; Huang, F. A Tutorial on Energy-Based Learning. *Predict. Struct. Data* **2006**, *1* (0).

(17) Hynes, J. T.; MUKHERJEE, A.; HRIDYA, V. Dynamical Recrossing in the Intercalation Process of the Anticancer Agent Proflavine into DNA. **2019**.

(18) Scherer, M. K.; Trendelkamp-Schroer, B.; Paul, F.; Pérez-Hernández, G.; Hoffmann, M.; Plattner, N.; Wehmeyer, C.; Prinz, J.-H.; Noé, F. PyEMMA 2: A Software Package for Estimation, Validation, and Analysis of Markov Models. *J. Chem. Theory Comput.* **2015**, *11* (11), 5525–5542.

(19) Chodera, J. D.; Swope, W. C.; Pitera, J. W.; Dill, K. A. Long-Time Protein Folding Dynamics from Short-Time Molecular Dynamics Simulations. *Multiscale Model. Simul.* **2006**, *5* (4), 1214–1226.

(20) Rethage, D.; Pons, J.; Serra, X. A Wavenet for Speech Denoising; IEEE, 2018; pp 5069–5073.

(21) Chekmarev, D. S.; Ishida, T.; Levy, R. M. Long-Time Conformational Transitions of Alanine Dipeptide in Aqueous Solution: Continuous and Discrete-State Kinetic Models. *J. Phys. Chem. B* **2004**, *108* (50), 19487–19495. <https://doi.org/10.1021/jp048540w>.

(22) Sasi kala, W. D.; Mukherjee, A. Molecular Mechanism of Direct Proflavine–DNA Intercalation: Evidence for Drug-Induced Minimum Base-Stacking Penalty Pathway. *J. Phys. Chem. B* **2012**, *116* (40), 12208–12212. <https://doi.org/10.1021/jp307911r>.

(23) Lundberg, S. M.; Lee, S.-I. A Unified Approach to Interpreting Model Predictions. In *Advances in Neural Information Processing Systems 30*; Guyon, I., Luxburg, U. V., Bengio, S., Wallach, H., Fergus, R., Vishwanathan, S., Garnett, R., Eds.; Curran Associates, Inc., 2017; pp 4765–4774.

(24) Lu, X.; Olson, W. K. 3DNA: A Software Package for the Analysis, Rebuilding and Visualization of Three-dimensional Nucleic Acid Structures. *Nucleic Acids Res.* **2003**, *31* (17), 5108–5121.

- (25) Gregor, K.; LeCun, Y. Learning Fast Approximations of Sparse Coding; 2010; pp 399–406.
- (26) Sasikala, W. D.; Mukherjee, A. Molecular Mechanism of Direct Proflavine–DNA Intercalation: Evidence for Drug-Induced Minimum Base-Stacking Penalty Pathway. *J Phys Chem B* **2012**, *116*, 12208.